Non-Newtonian Hele-Shaw Flow and the Saffman-Taylor Instability

Ljubinko Kondic,[1,*] Michael J. Shelley,[1] and Peter Palffy-Muhoray[2]
[1]*Courant Institute of Mathematical Sciences, New York University, New York, New York 10012*
[2]*Liquid Crystal Institute, Kent State University, Kent, Ohio 44242*
(Received 14 August 1997)

We explore the Saffman-Taylor instability of a gas bubble expanding into a shear thinning liquid in a radial Hele-Shaw cell. Using Darcy's law generalized for non-Newtonian fluids, we perform simulations of the full dynamical problem. The simulations show that shear thinning significantly influences the developing interfacial patterns. Shear thinning can suppress tip splitting, and produce fingers which oscillate during growth and shed side branches. Emergent length scales show reasonable agreement with a general linear stability analysis. [S0031-9007(97)05226-5]

PACS numbers: 47.50.+d, 47.20.Ma, 47.54.+r, 68.10.–m

Complex fluids, such as liquid crystals [1], polymer solutions and melts [2], clays [3], and foams [4], display rich non-Newtonian behavior—viscoelasticity, shear thinning and thickening, boundary or flow induced anisotropy—whose nonlinear effect on flow is understood at best phenomenologically. Hele-Shaw (H-S) flow between two closely spaced plates has been used to study such fluids; inertia is negligible, and the resulting description is simplified by the high aspect ratio geometry. Such "thin-gap" flows of non-Newtonian liquids are also relevant to industrial processes such as injection molding [5] and display device design [6]. Interest stems also from the close analogy between Newtonian H-S flow and quasistatic solidification; the Saffman-Taylor (S-T) instability of the driven fluid-fluid interface plays the same role as the Mullins-Sekerka instability of the solidification front [7]. Features usually associated with solidification, such as the growth of dendritic fingers and side branching, have also been observed in Newtonian fluids with imposed anisotropy, say by scoring lines on the cell plates [8]. However, experiments using non-Newtonian or anisotropic fluids have shown that solidification structures, such as snowflake patterns in liquid crystal flows [1], or needle crystals in polymeric solutions [2], can be induced by the bulk properties of the fluid itself, without any imposed anisotropy.

In [9], we conjectured that shear thinning—a property of polymeric liquids and effectively of nematic liquid crystals in certain geometries—was a crucial ingredient in suppressing tip splitting, and might lead to the appearance of dendritelike structures in complex fluids. In this scenario, the tip of a finger lies in a region of high shear, and thus lower viscosity, which causes it to advance with higher relative velocity than surrounding portions of the interface, suppressing the spreading of the tip. To study this, we derived from first principles a natural generalization of Darcy's law which takes into account shear thinning (or thickening) in an isotropic fluid. In support of our conjecture, we showed that for a gas bubble expanding into a *weakly* shear thinning fluid, the S-T instability is modified to give increased length-scale selection. In this Letter, we use the generalized Darcy's law to perform fully nonlinear simulations of a bubble expanding into a strongly shear thinning liquid. The simulations demonstrate that shear thinning significantly modifies the evolution of the interface, and can produce fingers whose tip splitting is suppressed, and which have dendritic appearance. The resulting patterns are often similar to those observed in experiments [1–4,10,11]. Length scales from our linear stability analysis are consistent with simulational results. Finally, we give a morphological phase diagram in terms of flow and fluid parameters.

Formulation.—Consider a gas bubble expanding under applied pressure into a non-Newtonian fluid in a radial H-S cell. The fluid domain is an annular region Ω with inner boundary Γ_i and external boundary Γ_e. Neglecting inertia, we use the Stokes equations with shear-rate dependent viscosity,

$$\nabla p = \nabla \cdot (\mu(|\mathbf{S}|^2)\mathbf{S}), \qquad \nabla \cdot \mathbf{v} = 0. \tag{1}$$

Here p is pressure, $\mathbf{S}$ is the rate-of-strain tensor for the fluid velocity $\mathbf{v}(x, y, z) = (u, v, w)$, with z the "short," cross-gap direction, and $|\mathbf{S}|^2 = tr(\mathbf{S}^2)$. We follow [12] and use the viscosity model $\mu(|\mathbf{S}|^2) = \mu_0 f_\alpha(\tau^2|\mathbf{S}|^2)$, with $f_\alpha(\xi^2) = (1 + \alpha\xi^2)/(1 + \xi^2)$. Here τ is the longest (Zimm) relaxation time of the fluid, μ_0 is its zero shear-rate viscosity, and α measures shear dependence: $\alpha = 1$ is Newtonian, $\alpha > 1$ gives shear thickening, and $\alpha < 1$ gives shear thinning. In practice, most non-Newtonian fluids are shear thinning.

The flow is simplified by the small aspect ratio $\epsilon = b/L \ll 1$, where L is a typical lateral length scale, and b is the plate separation. To nondimensionalize, the lateral and vertical distances are scaled by L and b, respectively. The scale for pressure is taken as $\bar{p}/\epsilon$, where $\bar{p}/\epsilon$ is the driving (gauge) pressure. The natural velocity and time scales are then $U_c = \epsilon L\bar{p}/\mu_0$ and $T_c = \mu_0/\epsilon\bar{p}$. This is the scaling required for shear thinning of the fluid to be apparent [13]. At leading order in ϵ, in [9] we derived from Eq. (1) a generalized Darcy's law for the gap averaged, lateral

velocity $\mathbf{u}$,

$$\mathbf{u} = \frac{-1}{12\bar{\mu}_\alpha(\mathrm{We}^2|\nabla p|^2)}\nabla p, \quad \text{and} \quad \nabla\cdot\mathbf{u} = 0, \qquad (2)$$

where now $\nabla = (\partial_x, \partial_y)$. $\mathrm{We} = \tau/\tau_{\mathrm{flow}}$ is a Weissenberg number, with τ_{flow} a typical inverse shear rate in the short direction. The viscosity $\bar{\mu}_\alpha$ is constructed from f_α, and shares its monotonicity properties; i.e., for a shear thinning fluid $\bar{\mu}_\alpha$ decreases with increasing argument. In other work on polymeric flows, Bonn and co-workers [12] have proposed a model where the viscosity depends upon squared velocity; their model follows from ours [9]. Finding $\bar{\mu}_\alpha$ uniquely requires that $\alpha > 1/9$ [9].

We have also derived Eq. (2), again with viscosity f_α, from the Johnson-Segalman-Oldroyd (JSO) viscoelastic fluid model for polymeric flows [14]. We find that the model includes normal stress differences, but no elastic response, so long as $\mathrm{We} \sim O(1)$. The details of this derivation will be presented elsewhere [13].

An additional dimensionless parameter is the capillary number, $\mathrm{Ca} = 12\mu_0\dot{R}_0R_0^2/(\gamma b^2)$, measuring the relative strength of capillary and viscous forces. Here γ is surface tension, with length and velocity scales now specified for the case of an expanding circular bubble of initial radius R_0 and velocity $\dot{R}_0$ (i.e., $\mathrm{We} = \tau\dot{R}_0/b$). While Ca and We are defined by their values at $t = 0$, they are easily understood in terms of measurable experimental quantities.

From Eq. (2), the pressure satisfies the nonlinear boundary value problem in Ω,

$$\nabla\cdot\left(\frac{\nabla p}{\bar{\mu}_\alpha(\mathrm{We}^2|\nabla p|^2)}\right) = 0, \qquad p|_{\Gamma_i} = 1 - \frac{\kappa_i}{\mathrm{Ca}}, \qquad p|_{\Gamma_e} = \frac{\kappa_e}{\mathrm{Ca}}, \qquad (3)$$

where the standard Young-Laplace boundary condition (κ is lateral curvature) is assumed at Γ_i and Γ_e. Using this simple boundary condition, we have ignored complicated flows in the neighborhood of the meniscus [15,16], and in the case of polymeric flows, the possibility of a stretch-coil transition [11]. Finally, the motion of the interfaces $\Gamma_{i,e}$ is given by the condition that they move with the fluid velocity.

Note that We can be removed from our dynamical system by the rescaling $(x, y) \to \mathrm{We}(x, y)$, $t \to \mathrm{We}^2 t$, and $\mathrm{Ca} \to \mathrm{Ca}/\mathrm{We}$. However, to retain a fixed physical length scale for our initial data, we retain a We dependence in what follows.

Linear stability analysis.—In Newtonian flow, the linear stability of an expanding circular bubble is determined by the capillary number Ca. The competition of capillary and driving forces gives an azimuthal wave number of maximum growth, $m_{\max}^{\mathrm{Newt}}$, with surface tension stabilizing short wavelengths. In [9], we derived an analytical expression for the growth rate in the limit of weak shear thinning: $\delta = 1 - \alpha \ll 1$. This showed that above a moderate Ca, shear thinning tightens the band of unstable modes, and can yield higher growth rates near $m = 0$. The mode of maximum growth is also shifted to lower wave numbers, $m_{\max} \approx m_{\max}^{\mathrm{Newt}}(1 - K\delta\,\mathrm{We}^2)$ (K a constant), and shorter wavelengths are further stabilized. This suggests enhanced length-scale selection, and supports the postulate that shear thinning can lead to suppression of tip splitting. These observations are consistent with Fig. 1(a), which shows numerically calculated growth rates. Figure 1(b) shows the length scale of the most unstable linear mode, as a function of Ca, in good agreement with the scaling $L \sim 1/\mathrm{Ca}^{1/2}$, which holds well for Newtonian fluids [17].

Simulation.—Equation (3) is much more difficult to solve than the analogous Newtonian problem, where the pressure is harmonic, and efficient boundary integral methods are available [18]. Here the pressure p satisfies a nonlinear elliptic equation which must be solved everywhere in Ω. Computations are done on a Lagrangian grid which conforms to and evolves with the interfaces. We use Newton's method to solve for the pressure. The requirements of high spatial resolution of the interface, coupled with time-stepping stability and accuracy constraints, produce a computationally intensive problem. To decrease this cost, a fourfold symmetric initial bubble shape is chosen, and this symmetry is enforced in the code.

Figure 2 shows the change in pattern formation as α decreases for fixed Ca and We ($\alpha = 1$ gives Newtonian flow for any We). The typical scenario for a Newtonian fluid is seen in Fig. 2(a). The initial shape is a circle perturbed by a $m = 4$ sine wave of amplitude a ($a/R_0 = 0.1$). Snapshots of the bubble at equal time intervals show growth

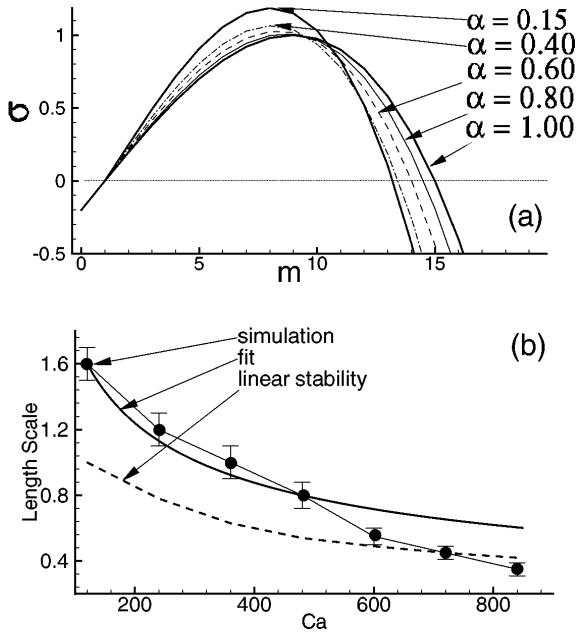

FIG. 1. (a) The growth rate σ_m for We = 0.15, Ca = 240. (b) For $\alpha = 0.15$, and We = 0.15, the length scale of the most unstable linear mode (dashed), and emergent length scale from simulations (dots). The solid curve is $A/\mathrm{Ca}^{1/2}$, where A is taken from the first data point.

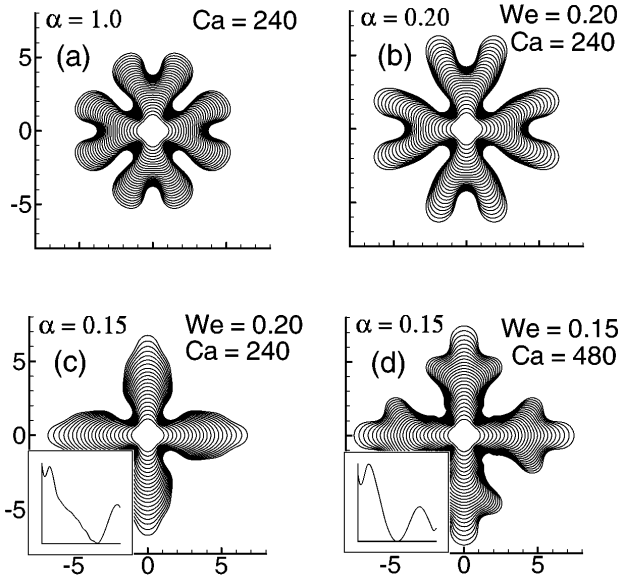

FIG. 2. The dynamics of bubble interfaces for a Newtonian fluid (a) and shear thinning fluids (b)–(d).

of the unstable fourth mode (in agreement with linear stability analysis) into a petal. The petal widens, then splits as its radius of curvature becomes larger than the wavelength of the unstable modes [17,18]. (This Newtonian simulation uses our general code; much longer simulations can be done using boundary integral methods [18].) In Fig. 2(b), with some shear thinning, there is delayed splitting of the tip, and the resulting fingers have reduced spreading. With greater thinning, Fig. 2(c) shows that even the initial splitting is suppressed, and the emergence of single fingers is seen. The inset plot shows tip curvature, which oscillates in time. While more apparent in Fig. 2(d), each oscillation is associated with the suppression of a nascent splitting, and produces side branches behind the propagating tip. Figure 2(d) shows the evolution for larger Ca and smaller We. Higher Ca enhances the growth of shorter wavelengths, and leads to more pronounced side branching. In this case, larger We gives an initial splitting.

Our patterns are very similar to those found in simulations of Newtonian H-S flow with anisotropic boundary conditions [19], as well as to local solidification models with anisotropy [20]. Recent experiments with foams [4] (where elastic properties might be of importance) and of polymeric liquids [2,10] can also produce patterns similar to our simulations.

To demonstrate how these structures are produced by shear thinning, and to substantiate our original postulate, Fig. 3 shows viscosity contours and velocity vectors of the flow in Fig. 2(d), at the last time shown. As expected, low viscosities at the finger tips enhance their velocity, while away from tips motion is suppressed. The fingers still show a tendency towards tip broadening due to the large driving pressure (large Ca). Likely it is the interplay of these effects which gives the curvature oscillations and

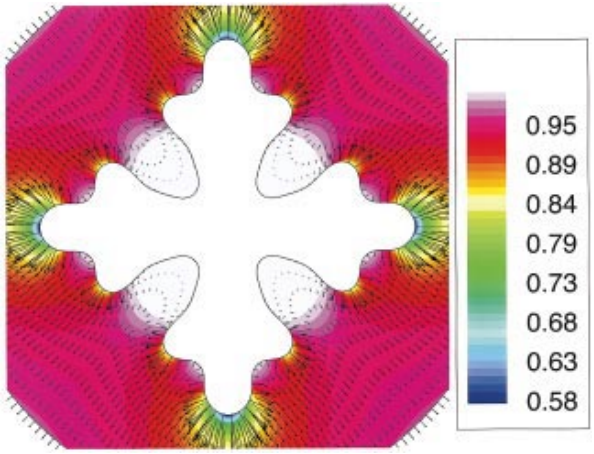

FIG. 3(color). Contour plot of the viscosity of the driven fluid and vector plot of its velocity (We = 0.15, $\alpha = 0.15$, Ca = 480).

side branching. The similarity to dendrites in solidification is striking, and while oscillating dendrites have been observed [21], their tips are typically stable, with constant curvature. More relevant are oscillations in propagating fingers observed in flows of dilute polymer solutions in a channel geometry [11], though these could be associated with a stretch-coil transition.

We have explored further the $(\mathrm{Ca}, \mathrm{We}, \alpha)$ parameter space. Figure 4 shows typical patterns in one slice ($\alpha = 0.15$). From such diagrams, we can formulate conditions for the suppression of tip splitting, and understand the influence of Ca, We, and α on the dynamics of the interface.

(i) To suppress tip splitting, the fluid has to be strongly shear thinning; small values of α yield narrow fingers, as in Figs. 2(c) and 2(d). For our initial data there is a

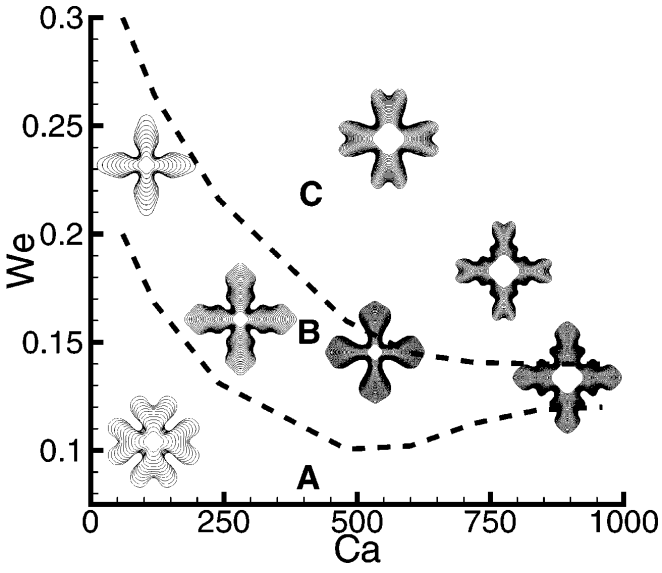

FIG. 4. Morphological phase diagram for pattern formation in a strongly shear thinning fluid ($\alpha = 0.15$).

critical value ($\alpha_{\text{crit}} > 0.25$) above which the initial petal always splits, independently of other parameters. This behavior is consistent with experiments with water based muds [3], where increased colloid concentration gives stronger shear thinning and yields narrowed fingers.

(ii) We determine which part of the viscosity curve governs the response of the fluid. Figures 2(c) and 2(d), where nonsplitting fingers are obtained, show a situation where viscosity varies considerably along the interface. This seems to be a necessary condition for suppression of tip splitting. There is a range in We for this behavior, and its size depends strongly on α; as α increases, this range of We decreases. Also, an increase of Ca shifts this window towards lower We (Fig. 4). And so, at increased pumping pressure, the fluid should have a shorter relaxation time if nonsplitting tips are to be observed. This effect has been observed in experiments with liquid crystals [22] where the driving pressure was varied: At low driving pressures, the pattern was Newtonian (corresponding here to small Ca and We—region *A* in Fig. 4). At intermediate driving pressures, the tips did not split (as in region *B*), and finally, even higher driving pressures (large Ca and We) resulted again in a tip splitting phase (as in region *C*). These observations agree very well with our results.

(iii) The increase of Ca has two effects. First, as in a Newtonian fluid, an increase of Ca excites shorter wavelengths, leading to shorter length scales; Fig. 1(b) shows length scales from our simulation, together with a fit of the form $A/\text{Ca}^{1/2}$. While it is not clear that this scaling is satisfied, there is reasonable agreement in magnitude with the linear theory. A decrease in finger width in a radial geometry was observed in some of the first experiments done with shear thinning fluids [23], where reducing the plate separation b gave a larger Ca, though this increases We as well. We find also that an increase of Ca above $\approx$500 narrows the range in We where fingers do not split (viz. Fig. 4).

Detailed experimental studies combined with sophisticated modeling are necessary for a detailed understanding of the flow behavior of complex fluids. In this Letter, we have shown that shear thinning alone can suppress tip splitting in a radial Hele-Shaw cell, and produce dendritic fingers. This agrees with preliminary experimental results with polyethylenoxide (PEO) solutions [24]. In our approach, we have neglected several potentially important effects. For very strongly shear thinning polymeric flows, there is the possibility of slip-layer formation, and of strong elastic response. In principle, these are accounted for within the JSO viscoelastic model, and have been the subject of theoretical work [25]. A more thorough understanding is needed of flows in the neighborhood of the interface, as has been reached for Newtonian H-S [15], and partially for viscoelastic [16] flows.

We thank Jens Eggers, Petri Fast, and Wim van Saarloos for useful discussions. This work was supported in part by NSF Grant No. DMS-9404554 (M. J. S.), ALCOM Grant No. DMR89-20147 and AFOSR MURI Grant No. F4962-97-1-0014 (P. P-M.), and DOE Grant No. DE-FG02-88ER25053 (M. J. S., L. K.).

*Present address: Departments of Mathematics and Physics, Duke University, Durham, NC 27708.

[1] A. Buka, P. Palffy-Muhoray, and Z. Racz, Phys. Rev. A **36**, 3984 (1987).
[2] H. Zhao and J. V. Maher, Phys. Rev. E **47**, 4278 (1993).
[3] H. Van Damme and E. Lemaire, in *Disorder and Fracture*, edited by J. C. Charmet, S. Roux, and E. Guyon (Plenum Press, New York, 1990).
[4] S. Park and D. Durian, Phys. Rev. Lett. **72**, 3347 (1994).
[5] C. A. Hieber, in *Injection and Compression Molding Fundamentals*, edited by A. I. Isayev (Marcel Dekker, New York, 1987).
[6] C. Z. Van Doorn, J. Appl. Phys. **46**, 3738 (1975).
[7] J. S. Langer, in *Statistical Physics*, edited by H. E. Stanley (North-Holland, Amsterdam, 1986).
[8] E. Ben-Jacob *et al.*, Phys. Rev. Lett. **55**, 1315 (1985).
[9] L. Kondic, P. Palffy-Muhoray, and M. J. Shelley, Phys. Rev. E **54**, R4536 (1996).
[10] M. Kawaguchi, K. Makino, and T. Kato, Physica (Amsterdam) **105D**, 121 (1997).
[11] D. E. Smith *et al.*, Phys. Rev. A **45**, R2165 (1992).
[12] D. Bonn, H. Kellay, M. Ben Amar, and J. Meunier, Phys. Rev. Lett. **75**, 2132 (1995); also D. Bonn *et al.*, Physica (Amsterdam) **220A**, 60 (1995).
[13] P. Fast, L. Kondic, and M. J. Shelley (to be published).
[14] R. G. Larson, *Constitutive Equations for Polymer Melts and Solutions* (Butterworth, Stoneham, 1988).
[15] G. M. Homsy, Annu. Rev. Fluid Mech. **1987**, 271 (1987); also D. Reinelt and P. Saffman, SIAM J. Sci. Stat. Comput. **6**, 542 (1985).
[16] J. Ro and G. Homsy, J. Non-Newton. Fluid Mech. **57**, 203 (1995).
[17] L. Paterson, J. Fluid. Mech. **113**, 513 (1981).
[18] T. Hou, J. Lowengrub, and M. Shelley, J. Comput. Phys. **114**, 312 (1994).
[19] S. K. Sarkar and D. Jasnow, Phys. Rev. A **39**, 5299 (1989); also R. Almgren, W. S. Dai, and V. Hakim, Phys. Rev. Lett. **71**, 3461 (1993).
[20] D. A. Kessler, J. Koplik, and H. Levine, Adv. Phys. **37**, 255 (1988).
[21] Y. Sawada, A. Dougherty, and J. P. Gollub, Phys. Rev. Lett. **56**, 1260 (1986).
[22] A. Buka, J. Kertesz, and T. Viscek, Nature (London) **323**, 424 (1986).
[23] J. Nittmann, G. Daccord, and H. E. Stanley, in *Fractals in Physics*, edited by L. Pietronero and E. Tosatti (North-Holland, Amsterdam, 1986).
[24] R. Ennis, P. Palffy-Muhoray, M. J. Shelley, and L. Kondic (to be published).
[25] D. Malkus, J. Nohel, and B. Plohr, SIAM J. Appl. Math. **51**, 899 (1991).